COMPUTATIONAL METHODS IN ENGINEERING
2nd Asia-Pacific Int. Conf. on Comp. Meth. in Engrg (ICOME 2006)
Nov. 14-16, 2006, Hefei, China

A Novel Approach to Analyse a Crack with the XFEM in Composite Media

S. Mohammadi [1]*, A. Asadpoure [2]

[1] *School of Civil Engineering, University of Tehran, Tehran, Iran*
[2] *Department of Civil Engineering, Sharif University of Technology, Tehran, Iran*

Email: smoham@ut.ac.ir

Abstract

A new approach is proposed to model a crack in orthotropic composite media using the extended finite element method (XFEM). The XFEM uses the concept of partition of unity in addition to meshless basic idea of approximating a field variable by its values at a set of surrounding nodes. As a result, higher order approximations can be designed with the same total number of degrees of freedom. In this procedure, by using meshless based ideas, elements containing a crack are not required to conform to crack edges. Therefore mesh generating is performed without any consideration of crack conformations for elements and the method has the ability of extending the crack without any remeshing. Furthermore, the type of elements around the crack-tip is the same as other parts of the finite element model and the number of nodes and consequently degrees of freedom are reduced considerably in comparison to the classical finite element method.

Keywords: Extended finite element method, orthotropic media, near tip field, crack.

INTRODUCTION

Since the strength to weight ratio of composite materials is higher than other conventional engineering materials, industrial and engineering applications of such materials have widely spread in recent years. Considering their strength, they are applied in the shape of thin layers while remain very imperfection sensitive. As a result, fracture behaviour of orthotropic materials has turned into an interesting active research subject. Some analytical investigation have been reported on the fracture behaviour of composite materials such as the pioneering one by Muskelishvili [1], Sih et al. [2], Tupholme [3], Viola et al. [4], Lim et al. [5] and Nobile and Carloni [6].

Owing to the fact that analytical methods are not considered as feasible methods for solving arbitrary problems, numerical methods such as the boundary element method, the finite element method, and meshless methods have been widely expanded and utilized in engineering applications. In many meshless methods, simulation of arbitrary geometries and boundaries is so cumbersome. However, the finite element method is more convenient and applicable because of its ability in modeling general boundary conditions, loadings, materials and geometries. One of its main drawbacks is that elements associated with a crack must conform to crack faces. Furthermore, remeshing techniques are required to follow crack propagation patterns. To improve these drawbacks in modeling discontinuities, Belytschko and Black [10] combined FEM with the partition of unity (proposed by Melenk and Babuška [11], Duarte and Oden [12]), soon to be known as the eXtended Finite Element Method (XFEM). In the XFEM, the finite element approximation is enriched with appropriate functions extracted from the fracture analysis around a crack-tip. The main advantage of the XFEM is its capability in modeling discontinuities independently, so the

mesh is prepared without considering the existence of discontinuities. In 2D isotropic media, Moës [13] and Dolbow [14] proposed an improvement to the work by Belytschko [10], and Sukumar [15] extended the method to 3D problems.

In the present study, a new set of enrichment functions is derived to simulate orthotropic cracked media using the extended finite element method. Crack-tip enrichment functions used in the extended finite element method are derived from already developed complex functions that determine the stress and displacement fields around a crack-tip. In this paper, first, essential formulations of orthotropic materials are reviewed. Then, the extended finite element method is concisely examined and the crack-tip (near-tip) enrichment functions are obtained. Thereafter, a method used for evaluating stress intensity factors is presented. Finally, in order to examine the robustness and validity of the proposed method, it is used to analyze various numerical examples and to evaluate mixed mode stress intensity factors and to compare them with available results.

ORTHOTROPIC MEDIA

Consider an orthotropic medium with axes of elastic symmetry co-incident with the Cartesian co-ordinates x-, y- and z-axes. The displacement component along the z-axis and all its derivatives with respect to z are assumed to be zero. The stress-strain equations can be defined as

$$\sigma_x = C_{11}\frac{\partial u}{\partial x} + C_{12}\frac{\partial v}{\partial y}\ ,\ \sigma_y = C_{12}\frac{\partial u}{\partial x} + C_{22}\frac{\partial v}{\partial y}\ ,\ \tau_{xy} = C_{33}\left(\frac{\partial u}{\partial y} + \frac{\partial v}{\partial x}\right) \tag{1}$$

where C_{ij} (i,j=1,2,3) are the relevant components of the compliance matrix of the material in x- and y-directions. Now the set of equations for an in-plane elastostatic problem can be expressed as

$$\frac{\partial^2 u}{\partial x^2} + \alpha\frac{\partial^2 u}{\partial y^2} + 2\beta\frac{\partial^2 v}{\partial x \partial y} = 0\ ,\ \frac{\partial^2 v}{\partial x^2} + \alpha_1\frac{\partial^2 v}{\partial y^2} + 2\beta_1\frac{\partial^2 u}{\partial x \partial y} = 0 \tag{2}$$

where

$$\alpha = \frac{C_{66}}{C_{11}},\quad \alpha_1 = \frac{C_{22}}{C_{33}},\quad \beta = \frac{C_{12}+C_{33}}{2C_{11}},\quad \beta_1 = \frac{C_{12}+C_{33}}{2C_{33}} \tag{3}$$

Following the methodology proposed by Viola et al. [4], a transformation is applied in order to express the formulation in terms of complex functions. Eqs. (2) can be represented by

$$\frac{\partial \mathbf{\Phi}}{\partial x} + \mathbf{A}\frac{\partial \mathbf{\Phi}}{\partial y} = \mathbf{0} \tag{4}$$

where

$$\mathbf{\Phi} = \left\{ \frac{\partial u}{\partial x}, \frac{\partial u}{\partial y}, \frac{\partial v}{\partial x}, \frac{\partial v}{\partial y} \right\}^T \tag{5}$$

$$\mathbf{A} = \begin{pmatrix} 0 & \alpha & 2\beta & 0 \\ -1 & 0 & 0 & 0 \\ 2\beta_1 & 0 & 0 & \alpha_1 \\ 0 & 0 & -1 & 0 \end{pmatrix} \tag{6}$$

Eigenvalues of the matrix **A** can be obtained by

$$\lambda^4 + 2a_1\lambda^2 + a_2 = 0 \tag{7}$$

with

$$a_1 = \frac{\left(\alpha + \alpha_1 - 4\beta\beta_1\right)}{2},\quad a_2 = \alpha\alpha_1 \tag{8}$$

where λ is the Eigen value of matrix **A**. Two types of orthotropic materials can be defined, $a_1 > \sqrt{a_2}$ (type I) and $|a_1| < \sqrt{a_2}$ (type II); based on the existence of the real part of the solution. The first type of orthotropic materials was studied by Asadpoure et al. [17], and only the type II is considered in this paper. The basic complex variables can then be written as

$$z_1 = \left(x - \frac{\gamma_1}{\gamma_1^2 + \gamma_2^2} y \right) + i\left(\frac{\gamma_2}{\gamma_1^2 + \gamma_2^2} y \right), \; z_2 = \left(x + \frac{\gamma_1}{\gamma_1^2 + \gamma_2^2} y \right) + i\left(\frac{\gamma_2}{\gamma_1^2 + \gamma_2^2} y \right) \tag{9}$$

where

$$\gamma_1 = \left[\frac{1}{2}\left(\sqrt{a_2} + a_1 \right) \right]^{1/2}, \; \gamma_2 = \left[\frac{1}{2} + \left(\sqrt{a_2} - a_1 \right) \right]^{1/2} \tag{10}$$

Now, consider an infinite orthotropic plate, consisting of a traction free line crack, which is subjected to uniform biaxial (T and kT) and shear (S) loads at infinity. Fig. 1 shows the crack geometry, loading conditions and the Cartesian and polar co-ordinates utilized in this study.

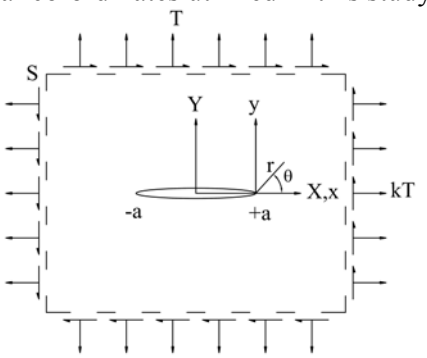

Fig. 1 Crack geometry, loading condition and global and local co-ordinates.

Neglecting the velocity of the crack propagation for the present static case, the basic solution proposed by Viola et al. [4] results in the following displacement fields in x ad y directions

$$\begin{aligned} u = & -2\beta\left[\left(p_3 A_1 - p^4 B_1 + p_4 B_2 \right) Y_1 + \left(p_3 B_1 + p_4 A_1 \right) X_1 + p_3 B_2 X_2 \right] \\ & + \frac{\beta T}{C_{33} D_1} \left\{ \left(p_3 k_6 + p_4 k_5 \right) \left[2\left(a + r\cos\theta \right) - \sqrt{2ar}\left(\sqrt{c_1(\theta)}\cos\theta_1/2 + \sqrt{c_2(\theta)}\cos\theta_2/2 \right) \right] \right. \\ & \left. - \left(p_3 k_5 + p_4 k_5 \right) \sqrt{2ar}\left(\sqrt{c_1(\theta)}\sin\theta_1/2 - \sqrt{c_2(\theta)}\sin\theta_2/2 \right) \right\} \\ & + \frac{\beta S}{C_{33} D_1} \left\{ \left(p_3 k_3 + p_4 k_4 \right) \left[X_1 - X_2 + \sqrt{2ar}\left(\sqrt{c_2(\theta)}\cos\theta_2/2 - \sqrt{c_1(\theta)}\cos\theta_1/2 \right) \right] \right. \\ & \left. - \left(p_3 k_4 + p_4 k_3 \right) \left[2Y_1 - \sqrt{2ar}\left(\sqrt{c_1(\theta)}\sin\theta_1/2 + \sqrt{c_2(\theta)}\sin\theta_2/2 \right) \right] \right\} \end{aligned} \tag{11}$$

$$\begin{aligned} v = & -\left[\left(\gamma_1 A_1 - \gamma_2 B_1 - \gamma_2 B_2 \right) Y_1 + \left(\gamma_2 A_1 + \gamma_1 B_2 \right) X_1 - \gamma_1 B_2 X_2 \right] \\ & + \frac{T}{2C_{33} D_1} \left\{ \left(\gamma_1 k_6 + \gamma_2 k_5 \right) \left[\left(X_1 - X_2 \right) + \sqrt{2ar}\left(\sqrt{c_1(\theta)}\cos\theta_2/2 - \sqrt{2ar}\cos\theta_2/2 \right) \right] \right. \\ & \left. + \left(\gamma_1 k_5 - \gamma_2 k_6 \right) \left[2Y_1 - \sqrt{2ar}\left(\sqrt{c_1(\theta)}\sin\theta_1/2 + \sqrt{c_2(\theta)}\sin\theta_2/2 \right) \right] \right\} \\ & + \frac{S}{2C_{33} D_1} \left\{ \left(\gamma_1 k_3 - \gamma_2 k_4 \right) \left[2\left(a + r\cos\theta \right) - \sqrt{2ar}\left(\sqrt{c_1(\theta)}\cos\theta_1/2 + \sqrt{c_2(\theta)}\cos\theta_2/2 \right) \right] \right. \\ & \left. + \left(\gamma_2 k_3 + \gamma_1 k_4 \right) \sqrt{2ar}\left(\sqrt{c_1(\theta)}\sin\theta_1/2 + \sqrt{c_2(\theta)}\sin\theta_2/2 \right) \right\} \end{aligned} \tag{12}$$

where

$$\begin{aligned} & p_1 + ip_2 = \frac{\left(\gamma_1 + i\gamma_2 \right)}{\alpha + \left(\gamma_1 + i\gamma_2 \right)^2}, \qquad p_3 + ip_4 = \left(\gamma_1 + i\gamma_2 \right)\left(p_1 - ip_2 \right) \\ & k_1 = \frac{C_{12} - 2\beta p_3 C_{11}}{C_{33}}, \qquad k_2 = 2\beta p_4 \frac{C_{11}}{C_{33}}, \; k_3 = \frac{C_{22} - 2\beta p_3 C_{12}}{C_{33}}, \qquad k_4 = 2\beta p_4 \frac{C_{12}}{C_{33}} \\ & k_5 = 2\beta p_2 - \gamma_2 \qquad , \qquad k_6 = 2\beta p_1 - \gamma_1 \end{aligned} \tag{13}$$

with

$$X_1 = (a + r\cos\theta) - \gamma_1 l^2 r\sin\theta \quad , \quad X_2 = (a + r\cos\theta) + \gamma_1 l^2 r\sin\theta$$
$$Y_1 = \gamma_2 l^2 r\sin\theta$$
$$A_1 = \frac{(k_3 k - k_1)T}{C_{33}(k_1 k_4 - k_2 k_3)} \quad , \quad D_1 = k_3 k_6 - k_4 k_5$$
$$B_1 = \frac{S}{2C_{33}k_6} + \frac{T}{2C_{33}k_6}\frac{[k(k_4 k_6 - k_3 k_5) + (k_1 k_5 - k_2 k_6)]}{(k_1 k_4 - k_2 k_3)} \tag{14}$$
$$B_2 = -\frac{S}{2C_{33}k_6} + \frac{T}{2C_{33}k_6}\frac{[k(k_4 k_6 - k_3 k_5) - (k_1 k_5 + k_2 k_6)]}{(k_1 k_4 - k_2 k_3)}$$

and

$$c_j(\theta) = \left(\cos^2\theta + l^2\sin^2\theta + (-1)^j l^2\sin 2\theta\right)^{1/2}, \quad l^2 = \left(\gamma_1^2 + \gamma_2^2\right)^{-1}, \quad j = 1,2. \tag{15}$$

$$\theta_j = arctg\left(\frac{\gamma_2 l^2\sin\theta}{\cos\theta + (-1)^j \gamma_1 l^2\sin\theta}\right), \quad j = 1,2. \tag{16}$$

It is noted that the displacement fields in Eqs. (11-12) are only valid for $\frac{r}{a} < 1$; near the crack-tip.

EXTENDED FINITE ELEMENT METHOD

X-FEM was originally proposed by Belytschko and Black [10] and Dolbow [14] and later modified and applied to various crack analysis problems by Sukumar et al. [15]. A numerical X-FEM model is constructed by dividing the model into two parts; first part is generating a mesh for the domain geometry (neglecting the existence of any crack or other discontinuities) and second part is enriching finite element approximation by appropriate functions for modeling any imperfections.

Consider **x** is a point of $\mathbf{R}^2$ (for 2-D space) or $\mathbf{R}^3$ (for 3-D space) in the finite element model and ***N*** is a set of nodes defined as $N = \{ n_1, n_2, ..., n_m \}$, m is the number of nodes in the element. The enriched approximation of displacement can be defined by:

$$\mathbf{u}^h(\mathbf{x}) = \underbrace{\sum_{\substack{I \\ n_I \in \mathbf{N}}} \phi_I(\mathbf{x})\mathbf{u}_I}_{\text{classical part of FEM}} + \underbrace{\sum_{\substack{J \\ n_J \in \mathbf{N}^g}} \phi_J(\mathbf{x})\psi(\mathbf{x})\mathbf{a}_J}_{\text{enriched part of FEM}} \tag{17}$$

where $\mathbf{u}_I$ is the classical nodal degree of freedom in FEM, $\mathbf{a}_J$ is the added set of degrees of displacement freedom to the standard finite element model, ϕ_I is the shape function associated to node *I*, $\psi(\mathbf{x})$ is the enrichment function and $\mathbf{N}^g$:

$$\mathbf{N}^g = \{ n_J : n_J \in \mathbf{N}, \omega_J \cap \Omega_g \neq \phi \} \tag{18}$$

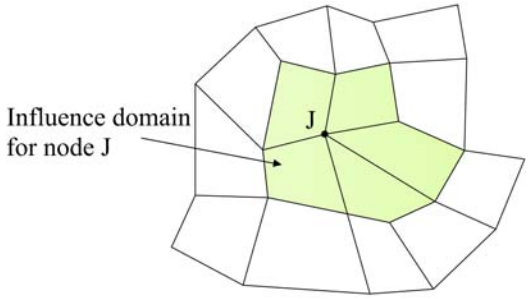

Fig. 2 Influence (support) domain for node J in an arbitrary finite element mesh

In Eq. (18), ω_J is the influence domain of ϕ_J for node n_J (Fig. 2) and Ω_g is the domain associated with a geometric entity such as crack surface, front, hole or any other discontinuities. According to the type of discontinouity, $\psi(\mathbf{x})$ can be chosen by applying its associated analytical solutions.

For modeling an arbitrary crack, Eq. (17) can be re-written as [14]:

$$\mathbf{u}^h(\mathbf{x}) = \sum_{\substack{I \\ n_I \in \mathbf{N}}} \phi_I(\mathbf{x})\mathbf{u}_I + \sum_{\substack{J \\ n_J \in \mathbf{N}^g}} \mathbf{b}_J \phi_J(\mathbf{x}) H(\mathbf{x}) + \sum_{k \in \mathbf{K}^1} \phi_k(\mathbf{x}) \left(\sum_l \mathbf{c}_k^{l1} \, \mathrm{F}_l^1(\mathbf{x}) \right) + \sum_{k \in \mathbf{K}^2} \phi_k(\mathbf{x}) \left(\sum_l \mathbf{c}_k^{l2} \, \mathrm{F}_l^2(\mathbf{x}) \right) \tag{19}$$

where $\mathbf{b}_J$ and $\mathbf{c}_k^l$ are vectors of additional nodal degrees of freedom, $\mathrm{F}_l^1(\mathbf{x})$ and $\mathrm{F}_l^2(\mathbf{x})$ are near-tip enrichment functions derived from the two-dimentional asymptotic dispalcement field near crack-tip and K^1 and K^2 are the set of nodes in which the crack-tip is in its suppurt domain for tip 1 and tip 2, respectively. $H(\mathbf{x})$ is the generalized Heaviside function which takes the value +1 if $\mathbf{x}$ is above the crack and –1, otherwise. If x^* is the nearest point on the crack to $\mathbf{x}$ and $\mathbf{e_n}$ is the unit vector normal to the crack alignment in which $\mathbf{e_s} \times \mathbf{e_n} = \mathbf{e_z}$ ($\mathbf{e_s}$ is the unit tangential vector), then:

$$H(\mathbf{x}) = \begin{cases} +1 & ;if\ (\mathbf{x} - \mathbf{x}^*).\mathbf{e_n} > 0 \\ -1 & ;otherwise \end{cases} \tag{20}$$

To select enriched nodes, the nodes that belong to K^1 or K^2 are enriched with the crack-tip enrichment function ($F_l(\mathbf{x})$) and those which contain the crack within their support domain and do not belong to K^1 or K^2 are enriched with Heaviside function ($H(\mathbf{x})$).

Crack-tip enrichment functions are obtained from the analytical solution for displacement in the vicinity of a crack-tip. These functions must span the possible displacement space that may be occurred in the analytical solution. Therefore, from Eqs. (11-12), it can be concluded that the functions having preceding properties are as

$$\{F_l(r,\theta)\}_{l=1}^4 = \left\{ \sqrt{r}\cos\frac{\theta_1}{2}\sqrt{c_1(\theta)}, \sqrt{r}\cos\frac{\theta_2}{2}\sqrt{c_2(\theta)}, \sqrt{r}\sin\frac{\theta_1}{2}\sqrt{c_1(\theta)}, \sqrt{r}\sin\frac{\theta_2}{2}\sqrt{c_2(\theta)} \right\} \tag{20}$$

where θ and $c_j(\theta)$ have been defined in equations (15) and (16).

In Eq. (20), the third and forth functions in the right-hand side of the equation are discontinuous across the crack faces while the others remain continuous.

The discrete system of linear equations in the XFEM in global form can be written as [16]

$$\mathbf{K}\mathbf{d} = \mathbf{f} \tag{21}$$

where $\mathbf{K}$ is the stiffness matrix, $\mathbf{d}$ is the vector of degrees of nodal freedom (for both classical and enriched ones) and $\mathbf{f}$ is the vector of external force. The global matrix and vectors are calculated by assembling matrices and vectors of each element. $\mathbf{K}$ and $\mathbf{f}$ for each element are defined as

$$\mathbf{k}_{ij}^e = \begin{bmatrix} \mathbf{k}_{ij}^{uu} & \mathbf{k}_{ij}^{ua} & \mathbf{k}_{ij}^{ub} \\ \mathbf{k}_{ij}^{au} & \mathbf{k}_{ij}^{aa} & \mathbf{k}_{ij}^{ab} \\ \mathbf{k}_{ij}^{bu} & \mathbf{k}_{ij}^{ba} & \mathbf{k}_{ij}^{bb} \end{bmatrix} \tag{22}$$

$$\mathbf{f}_i^e = \left\{ \mathbf{f}_i^u \quad \mathbf{f}_i^a \quad \mathbf{f}_i^{b1} \quad \mathbf{f}_i^{b2} \quad \mathbf{f}_i^{b3} \quad \mathbf{f}_i^{b4} \right\}^{\mathrm{T}} \tag{23}$$

where

$$\begin{aligned} \mathbf{k}_{ij}^{rs} &= \int_{\Omega^e} (\mathbf{B}_i^r)^{\mathrm{T}} \mathbf{D} \mathbf{B}_j^s \, \mathrm{d}\Omega \quad (r,s = u,a,b) \\ \mathbf{f}_i^u &= \int_{\partial\Omega_t^h \cap \partial\Omega^e} \varphi_i \bar{\mathbf{t}} \, \mathrm{d}\Gamma + \int_{\Omega^e} \varphi_i \mathbf{b} \, \mathrm{d}\Omega \\ \mathbf{f}_i^a &= \int_{\partial\Omega_t^h \cap \partial\Omega^e} \varphi_i H \bar{\mathbf{t}} \, \mathrm{d}\Gamma + \int_{\Omega^e} \varphi_i H \mathbf{b} \, \mathrm{d}\Omega \\ \mathbf{f}_i^{b\alpha} &= \int_{\partial\Omega_t^h \cap \partial\Omega^e} \varphi_i F_\alpha \bar{\mathbf{t}} \, \mathrm{d}\Gamma + \int_{\Omega^e} \varphi_i F_\alpha \mathbf{b} \, \mathrm{d}\Omega \quad (\alpha = 1,2,3 \text{ and } 4) \end{aligned} \tag{24}$$

where Ω^e is an element, Ω^h is an element with a crack lying along its edges, $\partial\Omega$ denotes the boundary of the domain $\Omega, \bar{\mathbf{t}}$ is the traction and **b** is the body force. In Eqs. (24), **B** is the matrix of shape function derivatives,

$$\mathbf{B}_i^u = \begin{bmatrix} \varphi_{i,x} & 0 \\ 0 & \varphi_{i,y} \\ \varphi_{i,y} & \varphi_{i,x} \end{bmatrix} \quad , \quad \mathbf{B}_i^a = \begin{bmatrix} (\varphi_i H)_{,x} & 0 \\ 0 & (\varphi_i H)_{,y} \\ (\varphi_i H)_{,y} & (\varphi_i H)_{,x} \end{bmatrix} \quad , \quad \mathbf{B}_i^\alpha = \begin{bmatrix} (\varphi_i F_\alpha)_{,x} & 0 \\ 0 & (\varphi_i F_\alpha)_{,y} \\ (\varphi_i F_\alpha)_{,y} & (\varphi_i F_\alpha)_{,x} \end{bmatrix} \quad (\alpha = 1,2,3 \text{ and } 4)$$

$$\mathbf{B}_i^b = \begin{bmatrix} \mathbf{B}_i^{b1} & \mathbf{B}_i^{b2} & \mathbf{B}_i^{b3} & \mathbf{B}_i^{b4} \end{bmatrix} \tag{25}$$

Because the ordinary Gaussian rules do not accurately calculate the integration of enrichment functions in elements cut by a crack, the element is subdivides into subquads. In this method, a node is enriched if there exist Gaussian points at both sides of the crack in the influence domain of the crack. Fig. 3 shows a mesh that contains a crack while the second method was applied. Although the crack cuts the element in Fig.3(a), node J must not be enriched because there is no Gaussian point above the crack. In contrary, node J in Fig. 3(b) has to be enriched.

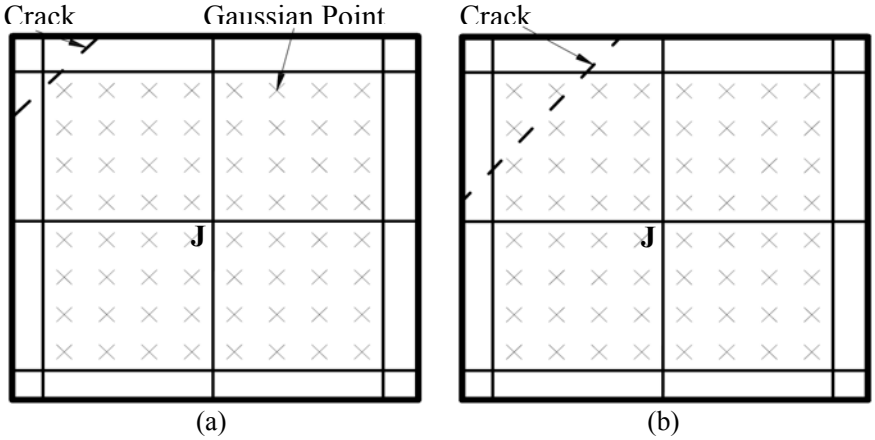

Fig. 3 (a) Node J is not enriched because Gaussian points of its support domain are not present at both sides of the crack, (b) node J must be enriched since there are Gaussian points at both sides of the crack.

NUMERICAL EXAMPLES

In this section some examples are presented. For comparing the results, Stress Intensity Factors (SIFs) and J-integral are calculated and compared. These parameters are among the best parameters for determination of the path of crack propagation. In this section, SIFs and J-integral are obtained by the method proposed by Kim and Paulino [16]. In the subsequent plane stress examples, the following parameters, being the function of independent engineering constants (E_{ij}, ν_{ij}, G_{ij}, i,j=1,2.), would be used

$$E = \sqrt{E_{11}E_{22}}, \quad \nu = \sqrt{\nu_{12}\nu_{21}}, \quad \delta^4 = \frac{E_{11}}{E_{22}} = \frac{\nu_{12}}{\nu_{21}}, \quad \kappa_0 = \frac{E}{2G_{12}} - \nu \tag{26}$$

where E is the efficient Young's modulus, ν is the effective Poisson's ratio, δ^4 is the stiffness ratio and κ_0 is the shear parameter. In all examples, elements containing a crack are partitioned into ten subquads and a 2×2 Gaussian rule is utilized for integrations in each one; while, a 2×2 Gaussian rule is applied in calculating regular finite element parameter.

1. Plate with a crack parallel to material axes of orthotropy

In this example, a crack aligned along the axis of orthotropy in the center of a plate is studied. At edges parallel to the crack, a fixed-grip loading or constant traction is applied. The constant stress is obtained by utilizing a uniform stress (σ=1) and the fixed-grip loading is obtained by a load equivalent to strain (ε_0=1) in the corresponding uncracked plate. Geometry and boundary conditions for the problem are illustrated in Fig. 4.

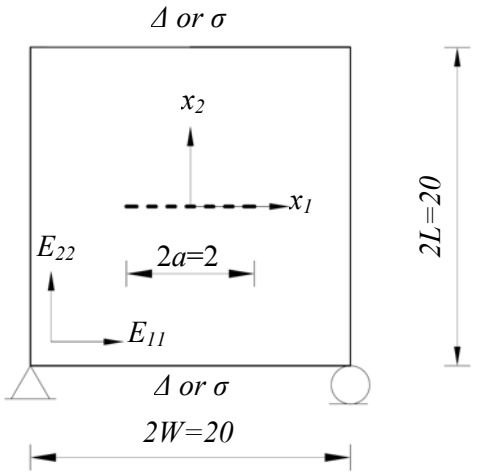

Fig. 4 Geometry and boundary conditions for a plate with a crack parallel to material axis of orthotropy.

In the FEM discretization, 2116 nodes with 2025 four-noded quadrilateral elements are used (Fig. 5). The size of crack-tip element is one-sixteenth of the crack length, i.e. $h_e/a = 1/8$. Stress intensity factors are calculated and compared with those reported by Kim and Paulino [16], using a total of 2001 elements and 5851 nodes, as shown in Table 1.

Table 2 shows the rate of convergence for various integration domain sizes (r_d) for enrichment with and without crack-tip enrichment functions. As provided in Table 2 small domain sizes can not be used without the inclusion of crack-tip enrichment functions and in order to compensate for the local effects of the crack-tip, larger domains are preferred.

By including crack-tip enrichment functions, higher rates of convergence are anticipated, even for smaller domain sizes around the crack-tip. Numerical results show that when $r_d/a = 0.5$, the values of SIFs are independent from the domain size.

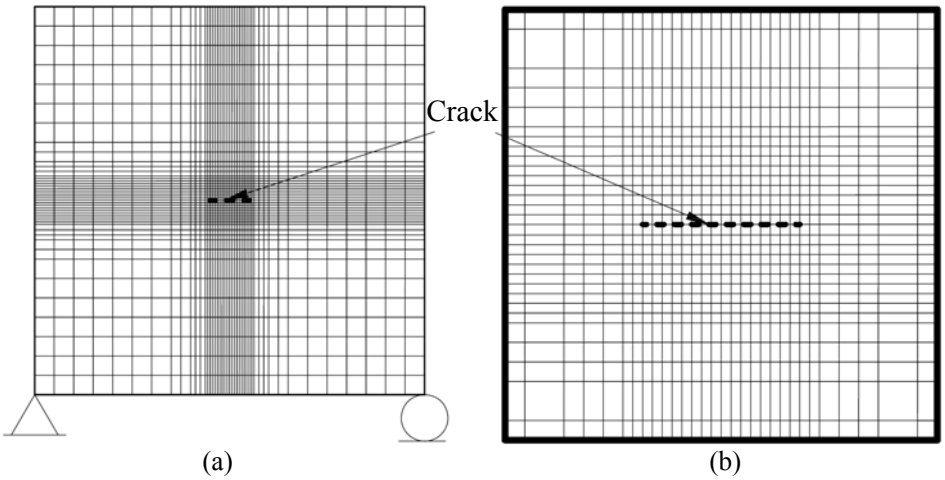

Fig. 5The discretizated model for a plate with a crack parallel to material axis of orthotropy, (a) whole view of FEM discretization model, (b) details of descretization around the crack-tip.

Table 1. Values of normalized SIFs for a plate with a crack parallel to material axis of orthotropy.

Method	$\overline{K_I}$	$\overline{K_{II}}$
Kim and Paulino [16]	0.997	0
Proposed method	1.018	0

$\overline{K_I} = K_I/\sigma\sqrt{\pi a}$ and $\overline{K_{II}} = K_{II}/\sigma\sqrt{\pi a}$ for the applied uniform stress

$\overline{K_I} = K_I\delta^2/\varepsilon_0 E\sqrt{\pi a}$ and $\overline{K_{II}} = K_{II}\delta^2/\varepsilon_0 E\sqrt{\pi a}$ for fixed-grip loading

Table 2. Comparison of normalized SIFs with and without crack-tip functions .

Relative domain size (r_d/a)	Without crack-tip function		With crack-tip function	
	$\overline{K_I}$	$\overline{K_{II}}$	$\overline{K_I}$	$\overline{K_{II}}$
0.25	0.966	0	1.018	0
0.5	1.014	0	1.017	0
1	1.015	0	1.017	0
2	1.016	0	1.018	0

$\overline{K_I} = K_I/\sigma\sqrt{\pi a}$ and $\overline{K_{II}} = K_{II}/\sigma\sqrt{\pi a}$ for the applied uniform stress

$\overline{K_I} = K_I\delta^2/\varepsilon_0 E\sqrt{\pi a}$ and $\overline{K_{II}} = K_{II}\delta^2/\varepsilon_0 E\sqrt{\pi a}$ for fixed-grip loading

Table 3. Comparison of normalized SIFs for the proposed and isotropic enrichment functions.

Number of Elements	Number of DOF	Proposed enrichment functions		Isotropic enrichment functions	
		$\overline{K_I}$	$\overline{K_{II}}$	$\overline{K_I}$	$\overline{K_{II}}$
2025	4278	1.018	0	1.021	0
784	1712	1.017	0	1.019	0
400	904	1.017	0	1.016	0

$\overline{K_I} = K_I/\sigma\sqrt{\pi a}$ and $\overline{K_{II}} = K_{II}/\sigma\sqrt{\pi a}$

To investigate the effect of number of elements in the numerical analysis, some coarser meshes are utilized and the results are given in Table 3. In this table, the results for SIFs are compared when isotropic enrichment functions (Dolbow [14]) and the proposed method are applied. As shown in Table 3, the results for both methods are different 0.2% and the values of the mode I stress intensity factors are more stable than the other one.

2. A single edge notched tensile specimen with crack inclination

The method proposed in this study is applied to a single edge notched tensile specimen. The material properties and geometry of the specimen are shown in Fig. 6. In this study, mixed mode stress intensity factors have to be evaluated because the crack has an inclination with respect to the line of symmetry. The finite element mesh of the model consists of 1920 4-noded quadrilateral element as shown in Fig. 7. The model has 14×40 fine elements with 0.075×0.075 Cm around the crack and 32×40 elements 0.075×0.15 cm far from the crack. For the numerical approach, a 2×2 Gauss quadrature is applied to evaluating classical finite element parameters, while for enriched nodes belong to elements that contain crack within their selves, elements are partitioned into 5 sections in both directions and in each section a 6×6 Gauss quadrature is utilized. The results are compared in Table 4. The calculated SIFs are based on the converged values corresponding to the case of eight elements far from the crack-tip position. The stress intensity factors reported by Jernkvist [18] were correlated to the load through the usual procedure of identifying displacements of nodal points on the crack surfaces close to the crack-tip by six crack inclinations φ in the range from 0° to 45°.

According to Table 4, while the stress intensity factors are only different within 1.1% and 7.9% for mode I, they are different within 0% to 5.1% for mode II. When the crack inclination is low, they are more similar

and the maximum differences for the two first inclinations are 1.1% and 0.6% for mode I and II, respectively.

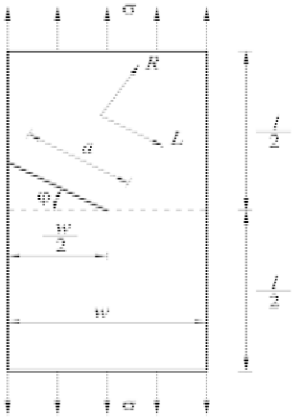

Elastic properties:
E_R=0.81 GPa; E_L=11.84 GPa
E_T=0.64 GPa; G_{LR}=0.63 GPa
v_{LR}=0.38 ; v_{LT}=0.56
v_{RT}=0.43

Fig. 6 Specimen geometry of a rectangular plate with single notched cracked.

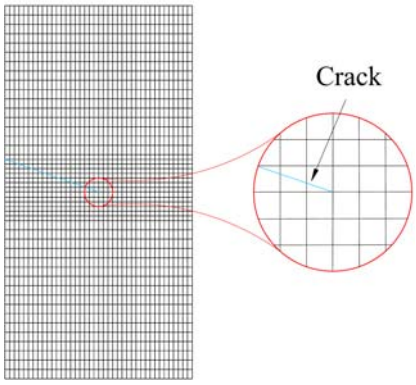

Fig. **7** Finite Element mesh for a single edge notched tensile specimen with crack inclination

Table 4. The effect of crack angle on the normalized stress intensity factor.

Φ (°)	Proposed method		Jernkvist [22]	
	$\frac{K_I}{\sigma\sqrt{\pi a}}$ (% *difference*)	$\frac{K_{II}}{\sigma\sqrt{\pi a}}$ (% *difference*)	$\frac{K_I}{\sigma\sqrt{\pi a}}$	$\frac{K_{II}}{\sigma\sqrt{\pi a}}$
0	2.960 (2.2)	0.0 (0.0)	3.028	0.0
15	3.000 (1.1)	0.361 (0.6)	3.033	0.359
30	3.120 (3.3)	0.691 (0.9)	3.020	0.685
45	3.029 (7.9)	0.908 (5.1)	2.806	0.864

CONCLUSION

The problem of modeling crack in orthotropic media was studied. The extended finite element method was adopted for modeling the crack and analyzing the domain numerically. In the extended finite element method, first the finite element model without any discontinuities is created and then the two-dimensional asymptotic crack-tip displacement fields with a discontinuous function are added to enrich the finite element approximation using the framework of partition of unity. The main advantage is the ability of the method in taking into consideration the crack without any explicit meshing of the crack surfaces, and the growth of any crack can readily be applied without any remeshing. The analytical solution for the displacement is applied to obtain the two-dimensional asymptotic crack-tip functions. Mixed-mode stress intensity factors (SIFs) were evaluated to determine the fracture properties of domain. The results obtained

by the proposed method are in good agreement with other available numerical or (semi-) analytical methods. In most examples, the maximum difference between the developed method and other available methods is about 1.7% for mode I and 2.4% for mode II. Numerical results depict that values of stress intensity factors are independent from the domain size as the domain size reaches to 0.325 of the crack length.

REFERENCES

1. Muskelishvili NI. Some basic problems on the mathematical theory of elasticity, Noordhoof, Groningen, 1952.
2. Sih GC, Paris PC, Irwin GR. On cracks in rectilinearly anisotropic bodies. International Journal of Fracture Mechanics **1** (1965), 189–203
3. Tupholme GE. A study of cracks in orthotropic crystals using dislocations layers. Journal of Engineering and Mathematics **8** (1974), 57–69.
4. Viola A, Piva A, Radi E. Crack propagation in an orthotropic medium under general loading. Engineering Fracture Mechanics **34**(5) (1989), 1155-1174.
5. Lim WK, Choi SY, Sankar BV. Biaxial load effects on crack extension in anisotropic solids, Engineering Fracture Mechanics **68** (2001), 403–416.
6. Nobile L, Carloni C. Fracture analysis for orthotropic cracked plates, Composite Structures **68**(3) (2005), 285-293.
7. Cruse T. Boundary Element Analysis in Computational Fracture Mechanics, Kluwer: Dordrecht, 1988.
8. Swenson D, Ingraffea A. Modeling mixed mode dynamic crack propagation using finite elements: Theory and applications. Comput. Mech. **3** (1988) 381-397
9. Belytschko T, Lu YY, Gu L. Element-free Galerkin methods. International Journal for Numerical Methods in Engineering **37** (1994) 229-256
10. Belytschko T, T. Black T. Elastic crack growth in finite elements with minimal remeshing, Int, J, Num, Meth, Engng. **45** (1999), 601- 620.
11. Melenk JM, Babuška I. The partition of unity finite element method: basic theory and applications, Computer Methods in Applied Mechanics and Engineering **139** (1996), 289–314
12. Duarte CA, Oden JT. An H-p adaptive method using clouds, Computer Methods in Applied Mechanics and Engineering **139** (1996), 237–262.
13. Moës N, Dolbow J, Belytschko T, A finite element method for crack growth without remeshing, International Journal for Numerical Methods in Engineering **46** (1999), 131–150.
14. Dolbow J, An Extended Finite Element Method with Discontinuous Enrichment for Applied Mechanics, Theoretical and Applied Mechanics, Northwestern University, Evanston, IL, USA: Ph.D. thesis, 1999
15. Sukumar N, Moës N, Moran B, Belytschko T. Extended finite element method for three-dimensional crack modeling, International Journal for Numerical Methods in Engineering **48** (2000), 1549–1570
16. Kim JH, Paulino GH. The interaction integral for fracture of orthotropic functionally graded materials: evaluation of stress intensity factors, International Journal of Solids and Structures **40** (2003), 3967-4001
17. Asadpoure A, Mohammadi S, Vafai A. Crack analysis in orthotropic media using the extended finite element method, submitted for publication
18. Jernkvist LO. Fracture of wood under mixed mode loading II Experimental investigation of Picea abies. *Engineering Fracture Mechanics* 2001; **68**:565-57